Preprint Cambridge Centre for Computational Chemical Engineering ISSN 1473 – 4273

Surface chemistry and particle shape. Processes for the evolution of aerosols in Titan's atmosphere

Panayotis Lavvas [1], Markus Sander [2], Markus Kraft [2] and Hiroshi Imanaka [1]

released: 17 September 2010

[1] Lunar and Planetery Laboratory, University of Arizona, Tucson, USA

[2] Department of Chemical Engineering and Biotechnology
University of Cambridge
New Museums Site
Pembroke Street
Cambridge, CB2 3RA
UK
E-mail: mk306@cam.ac.uk

Preprint No. 98

Keywords: soot, Titan, particle

Edited by
Computational Modelling Group
Department of Chemical Engineering and Biotechnology
University of Cambridge
New Museums Site
Cambridge CB2 3RA
United Kingdom

Fax: + 44 (0)1223 334796
E-Mail: c4e@cam.ac.uk
World Wide Web: http://como.ceb.cam.ac.uk/

Abstract

We use a stochastic approach in order to investigate the production and evolution of aerosols in Titan's atmosphere. The simulation initiates from the benzene molecules observed in the thermosphere and follows their evolution to larger aromatic structures through reaction with gas phase radical species. Aromatics are allowed to collide and provide the first primary particles, which further grow to aggregates through coagulation. We also consider for the first time the contribution of heterogenous processes at the surface of the particles, which are described by the deposition of the formed aromatic structures on the surface of the particles, and also through the chemical reaction with radical species. Our results demonstrate that the evolution of aerosols in terms of size, shape, and density is a result of competing processes between surface growth, coagulation and sedimentation. Furthermore, our simulations clearly demonstrate the presence of a spherical growth region in the upper atmosphere followed by a transition to an aggregate growth region below. The transition altitude ranges between 500 and 600 km based on the parameters of the simulation.

Contents

1 Introduction

The prominent aerosol layers on Titan result from the complex photochemistry in the satellite's atmosphere. Dissociation of the main atmospheric gas composition, dominantly by energetic photons and photoelectrons, initiates the growth of organic molecules, the increasing complexity of which, eventually yields the observed aerosols. These particles interact strongly with the solar radiation field, as demonstrated by the wavelength variation of Titan's geometric albedo, and by the observed stratospheric temperature increase concurrent with the main aerosol layer. But the most prominent aerosol signature is the almost featureless appearance of Titan's disk in visible wavelengths, due to the screening of the satellite's surface by the aerosols.

The size and shape of the aerosols initially perplexed researchers; Voyager and Pioneer measurements of polarized scattered light from altitudes probing the main haze layer (below 300 km) suggested that the particles have an average size of 0.15 μm [44, 51]. On the other hand, the observed high-phase angle scattering of the main haze layer, required particles of larger size, close to 0.5 μm [33]. In order to reconcile the two different sizes, [52] suggested that the aerosols in the main haze layer are aggregates composed of small spherical particles (the primary particles), with the latter responsible for the observed high degree of polarization, and the former providing the scattering at visible wavelengths. Theoretical calculations for the optical properties of aggregate particles, are consistent with the observed geometric albedo of Titan's disk, providing further support to this scenario [35]. The aggregates in these calculations have fractal properties characterized by a fractal dimension of 2 ([36] and references therein). The formation of aggregate particles is considered to take place outside the aerosol production region. Since the main aerosol layer is in the stratosphere most of the previous aerosol models assume a production region at a higher altitude, usually at 400 km (right above the detached haze layer observed at 350 km in Voyager images).

The DISR instrument of the Cassini/Huygens mission provided the first *in situ* observations of Titan's aerosols. The retrieved particle phase functions verified their strong forward scattering, which indisputably prove their aggregate structure [45]. In addition, observations by the Cassini UVIS and ISS instruments reveal the presence of a detached haze layer at ∼520 km, while aerosols were detected all the way to the thermosphere [23]. The optical properties of the aerosols below the detached layer corresponded to aggregate particles, as observed by DISR in the stratosphere, but above this altitude region the aerosol optical properties were characteristic of spherical particles. This lead [20] to suggest that the detached haze layer observed by the Cassini instruments corresponds to a transition region where the particle growth changes from spherical- to aggregate-type.

The presence of aerosols above 500 km suggests that the production must be at a higher altitude. Based on energy deposition considerations, the production of aerosols must initiate in the thermosphere since at this region photons able to dissociate N_2 and CH_4 deposit their energy, while lower energy photons penetrate deeper in the atmosphere below the detached haze layer [20, 21]. The thermospheric production argument is further supported by the CAPS/ELS detection of large negative

ions close to 1000 km with masses between 1000 and 10000 amu, which are representative of aerosols [7], but also by the surprisingly rich inventory of hydrocarbon and nitrogen containing species detected by INMS in the thermosphere as cations [47]. The INMS detection was limited up to masses of 100 amu, but the lower mass resolution observations of CAPS/IBS detected positive ions up to about 300 amu [8, 50]. These observations reveal a continuous growth of the chemical species towards larger masses, which eventually blends with the aerosols detected in the negative mode. This is a clear indication both for the photochemical production of Titan's aerosols and for their thermospheric origin.

Our understanding for the pathways leading to the observed aerosols is still at a preliminary stage. With the multitude of species observed in the thermosphere by INMS and the almost continuous distribution of masses in CAPS/IBS spectra it is reasonable to expect that aerosols are not a result of a single chemical process, but a result of multiple processes acting simultaneously and covering the total "phase space" of possible chemical products, based on the abundance of the gaseous species and their reactivity. Nevertheless, specific families of possible pathways can be identified based on the structure and composition of the reactant species. On these premisses, [18, 19, 22, 53] suggested specific aerosol production pathways from the gas phase background corresponding to pure hydrocarbon products, pure nitrile products, products of aromatic structure, and products that result from hydrocarbon and nitrile species reactions. The latest calculations show that some of these pathways have an important contribution in the aerosol production of the upper atmosphere. Since we do not yet know precisely all the mechanisms that lead from the gas-phase chemistry to the aerosols, we need to make some assumptions in our calculations. Here we consider the pathways related to the growth of polycyclic aromatic compounds (PACs). This is supported by the large abundance of benzene, the simplest aromatic hydrocarbon, observed in Titan's thermosphere [48, 50].

Apart from the production region, our understanding for the particle shape evolution is also preliminary. There is a common assumption among microphysical models that once the particles are formed from the background photochemistry they cease to interact with the gas phase molecules. Yet, recent investigations related to soot formation in flames has shown that under specific conditions the chemistry at the surface of the soot particles can significantly affect their size and structure [26, 27]. Although these experiments correspond to conditions very far from those present in Titan's atmosphere, we investigate here the possible role of surface chemistry in Titan's aerosols. The neutral chemistry in Titan's atmosphere is mainly driven by radical addition to closed cell molecules. Radicals, formed by the photolysis of closed cell molecules, are very reactive since they have energies larger than most of the potential barriers present in the reaction of two close cell molecules. Furthermore, radicals originating from highly unsaturated molecules (e.g. alkynes such as acetylene) are more reactive than radicals of saturated molecules (e.g. alkanes such as ethane). Based on photochemical models (e.g. [19]), a large number of radicals are available in Titan's atmosphere. Here, we investigate the interaction of some of these radicals with the aerosol surface.

In our investigation we use a stochastic approach to follow the evolution of particles

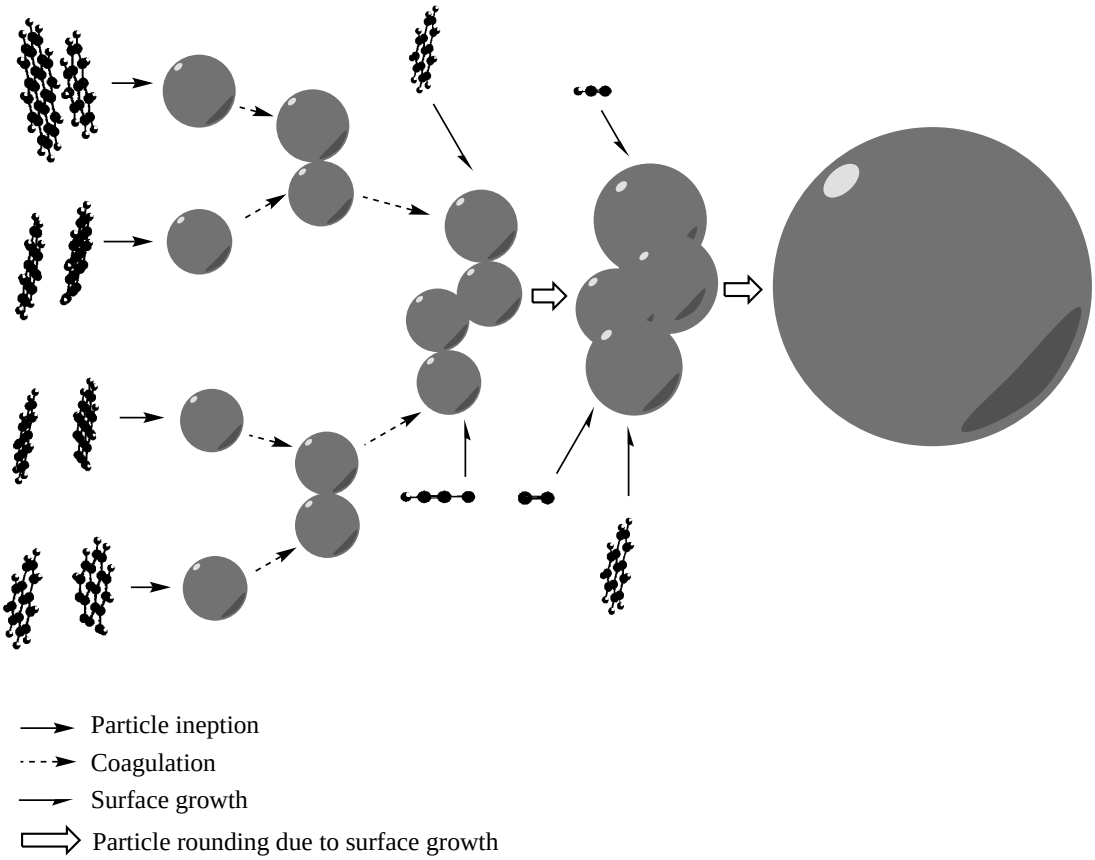

Figure 1: *Processes included in the model. In this example the PACs provide primary particles which then coagulate to form an aggregate. Eventually the surface chemistry acting on the aggregate provides a new, larger primary particle.*

through coagulation and surface chemistry, by simulating all growth stages from benzene molecules to PACs, to primary particles, and eventually aggregates. The stochastic particle model is able to simulate a multivariate particle population [3]. A high dimensional state space can be used to describe the particles and consequently a detailed chemical and structural information of each particle can be stored [5, 46]. Consequently the rounding of the particles can be simulated on a very detailed level [39]. The simulation speed is increased by taking advantage of the majorant rate approach [10, 12] and the linear process deferment algorithm developed by Patterson et al [29]. A similar model has already been successfully applied to model the sintering of silica nanoparticles [40] and the formation of soot in flames [39]. The model is described in detail in the following section. Our results for Titan's aerosols suggest that the surface chemistry is an important parameter in the growth of the particles and affects their size, shape and density.

2 Model Description

In order to simulate the coagulation of the particles in tandem with the impact of surface chemistry we use a stochastic approach that allows tracking the evolution of a particle assemble, from the initial chemical species to the final aggregate structures [38, 40, 41]. The starting point of the simulation are the benzene molecules, which are detected at high abundance in Titan's thermosphere [48]. These are allowed to grow to PACs through chemical reaction with radicals. There are two types of particles considered in the calculations: primary particles that are spherical, and aggregates of primary particles. Coagulation among primary particles provides aggregates, while surface chemistry can transform an aggregate to a larger primary particle. Different aspects of the calculations are discussed in detail below.

2.1 Stages of particle growth

The different processes included in the model are summarized in Fig. 1. We consider the collision of two PACs, leading to an adduct, to create a spherical primary particle with the mass of the two colliding PACs. The collision of two PACs is not always successful and we use an empirical formula that depends on the mass of the colliding PACs to describe the sticking efficiency [2, 34]. We assume a typical mass density of 1 g cm^{-3} for the primary particles. The coagulation of two primary particles provides an aggregate. The two colliding primary particles are in point contact directly after the coagulation event, but the neck at the touching point disappears and the aggregate gets rounder due to surface growth from the interaction with gas phase molecules and PAC deposition. The aggregates can further grow by coagulation with other primary particles or aggregates, and by surface growth.

An aggregate, $P = P(p_1, p_2, ..., p_n, \mathbf{S})$, composed of n primary particles is represented by a matrix $\mathbf{S}$ and primary particles p_i, which in turn are characterized by a volume v_i,

$$p_i = p_i(v_i) \quad i = 1, ..., n. \tag{1}$$

The quadratic and symmetric matrix $\mathbf{S}$ stores the common surface of each pair of two neighboring primary particles

$$\mathbf{S} = \begin{pmatrix} S_{11} & \cdots & S_{1n} \\ \vdots & \ddots & \vdots \\ S_{n1} & \cdots & S_{nn} \end{pmatrix}. \tag{2}$$

The dimension of $\mathbf{S}$ is the number of primary particles n present in the particle. The matrix element $S_{a,b}$ is the common surface of primary particles p_a and p_b if they are neighboring and is zero if the primaries are not neighbors. We use $\mathbf{S}$ to calculate the coalescence level $C(a, b)$ between each pair of neighboring primary particles, described below.

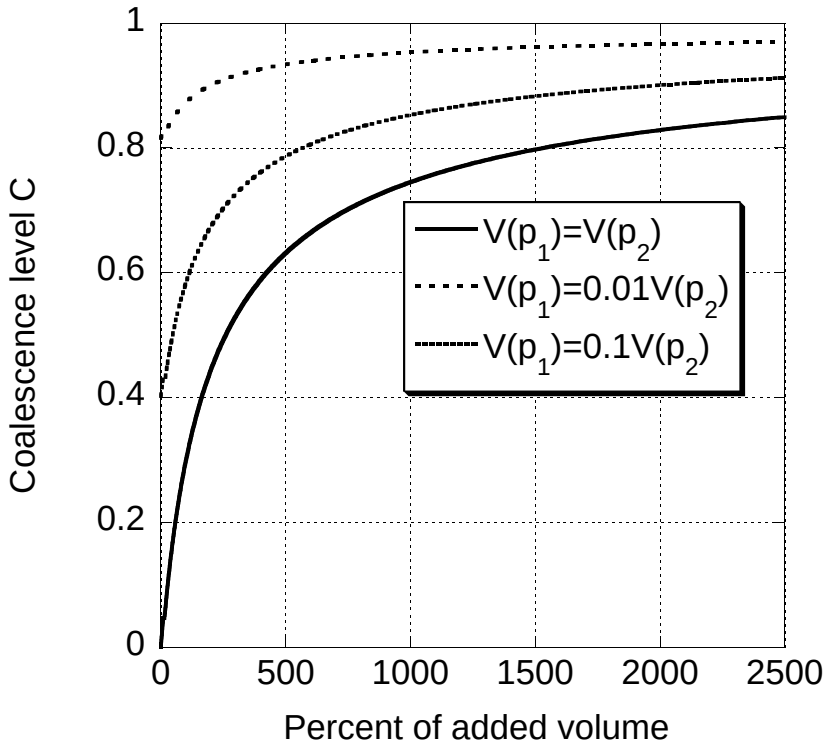

Figure 2: *Coalescence level $C(1,2)$ of two neighboring primary particles p_1 and p_2 as a function of the volume added relative to the sum of initial volume of the two primaries. Three different initial volume relations are compared*

2.2 Particle Rounding

Two primary particles, p_a and p_b, are in point contact directly after a collision. The initial common surface $S_{a,b}$ and volume $V_{a,b}$ of these two connected primary particles is the sum of the individual surfaces and volumes. The particles get more spherical due surface growth and can coalesce to one single primary particle. We calculate the coalescence level, $C(a,b)$, between two touching primaries p_a and p_b from [39]:

$$C(a,b) = \frac{\frac{S_{sph}(a,b)}{S_{a,b}} - 2^{-1/3}}{1 - 2^{-1/3}}, \tag{3}$$

where $S_{sph}(a,b)$ is the spherical surface (the surface of a sphere with the same volume as the two primary particles) and the matrix element $S_{a,b}$ is the common surface of the two neighboring primary particles p_a and p_b. $C(a,b)$ is zero directly after a coagulation event for two same volume particles, and is greater than zero if p_a and p_b have a different volume (Fig. 2). The mass deposited at the common surface of the two primary particles in contact, controls their volume change $\Delta V_{a,b}$, assuming a mass density of 1 g cm^{-3}. The corresponding increase in surface area, $\Delta S_{a,b}$, is calculated from [30]:

$$\Delta S_{a,b} = \Delta V_{a,b} \frac{s}{R_c}, \tag{4}$$

where the radius of curvature, R_c, is the radius of a sphere with the volume of the two connected primary particles. A smoothing factor of s=2 implies that the common surface $S_{a,b}$ increases as if the two primary particles would be spherical [30]. Smaller values of s lead to faster rounding of the particles. The coalescence level $C(a,b)$ increases due to surface growth and two individual primary particles are replaced by one primary particle if $C(a,b)$ is larger than 0.99. We assume that the rounding of the primary particles is independent from each other, which means that a coalescence event between primary particle p_a and p_b does not affect the coalescence level between primary particle p_a and p_c. In order to ensure this independence, the common surface $S_{a,b}$ of p_a and p_c is modified in such a way that their coalescence level does not change due to the coalescence of primary particle p_a and p_b [39].

2.3 Fractal Dimension

The particle shape is an important property for their physical properties (settling velocity, optical properties) and can be described by a fractal dimension, D_f, that correlates the number of primary particles n, with their distribution around the mass center of the aerosol:

$$n = k_f \left(\frac{R_g}{r_p} \right)^{D_f}, \tag{5}$$

where R_g the radius of gyration of the aerosol, r_p the average radius of the primary particles and k_f a proportionality constant of unit order (here we assume k_f=1). The radius of gyration is defined by:

$$R_g = \sqrt{\frac{\sum_{i=1}^{N} m_i r_i^2}{m_T}}, \tag{6}$$

where m_T is the total mass of the aggregate and m_i the mass of primary particle i whose center is at a distance r_i of the center of mass.

2.4 Growth rates

We use the brownian kernel for the calculation of the coagulation rates. Depending on the pressure conditions, the kernel approaches the slip-flow (high pressure), K^{sf}, and free molecular (low pressure), K^{fm}, limits. For intermediate pressures the kernel in the transition regime, K^{tr}, is calculated as the harmonic mean of the two limiting cases [32]:

$$K^{tr}(A,B) = \frac{K^{sf}(A,B)K^{fm}(A,B)}{K^{sf}(A,B) + K^{fm}(A,B)} \tag{7}$$

with A and B the two colliding members that can be particles, aerosols and PACs. For collision between PACs the sticking efficiency is calculated based on the mass and diameter of the smaller PAC [34], while for collisions among particles we take into account the possible charge at the particles for the sticking efficiency [21].

For primary particle inception by two PACs and for addition of PACs on particles (PAC deposition), we calculate the collision diameter of the PACs from:

$$d_c^{PAC} = d_A\sqrt{\frac{2n_c}{3}} \tag{8}$$

where $d_A = 1.395\sqrt{3}$Å for a single aromatic ring and n_c is the number of carbon atoms in the PAC [11].

For coagulation between aggregates, or primary particles and aggregates, the collision diameter of the aggregate, d_c^{part}, is calculated from:

$$d_c^{part} = \left(\frac{6V}{A_{part}}\right)\left(\frac{A_{part}^3}{36\pi V^2}\right)^{\frac{1}{D_f}} \tag{9}$$

where V is the aggregate volume and A_{part} its surface. The aggregate volume is calculated as the sum of the individual primary particles volume. The surface area of the aggregate incorporates the average coalescence level of the individual primary particles and is approximated by:

$$A_{part} = \frac{A_{sph}}{(C_{avg}(1-n^{-1/3}) + n^{-1/3})} \tag{10}$$

where A_{sph} is the spherical surface and C_{avg} the average coalescence level of the aggregate. This formula interpolates the surface between a coalescence level of zero, where the surface area is the sum of the individual primary particles, and a coalescence level of one, where the particle is spherical and consequently the surface area is equal to that of a sphere. Two colliding aggregates P_i and P_j do not change shape,

but stick together creating a bigger particle, P_k containing the primary particles of the two colliding particles:

$$P_i(p_1, ..., p_m, \mathbf{S}(P_i)) + P_j(p_1, ..., p_n, \mathbf{S}(P_j)) \rightarrow P_k(p_1, ..., p_{n+m}, \mathbf{S}(P_k)). \tag{11}$$

A primary particle p_a from particle P_i and a particle p_b from particle P_j are assumed to be the touching point of the two colliding particles. The matrix $\mathbf{S}$ of the resulting larger aerosol incorporates the two primaries p_a and p_b in contact:

$$\begin{pmatrix} & & \vdots & \\ & \mathbf{S}(P_i) \quad \cdots \quad S_{b,a} & & \cdots \\ & \vdots & \vdots & \\ \cdots & S_{a,b} \quad \cdots & \mathbf{S}(P_j) & \\ & \vdots & & \end{pmatrix}. \tag{12}$$

For the interaction of gas phase species with the surface of particles we calculate the growth rate from:

$$k_{gas} = \frac{1}{4} V_{th}^g N_g S_p a_s \tag{13}$$

where V_{th}^g and N_g is the thermal velocity and number density of the gas species, a_s its sticking efficiency and S_p the surface area of the particle. For the growth of individual PACs we follow the total number of C atoms added assuming the same reaction rate as for addition of the chemical species on a benzene molecule:

$$PAC(C_x) + C_k N_l \rightarrow PAC(C_{x+k+l}) \tag{14}$$

The chemical reaction rate used for the last reaction depends on the gas species used in the calculations. These are discussed below in the application of the model to Titan's conditions.

2.5 Particle sedimentation

The stochastic approach tracks the time evolution of an initial sampling volume. This volume corresponds to both PACs (including the initial benzene molecules) and primary particles/aerosols formed as time evolves. As the simulation evolves the volume sediments with a characteristic velocity that depends on the size and structure of the volume components. For spherical and aggregate particles we calculate the sedimentation velocity with the method described in [21]. For a PAC we calculate the settling velocity assuming a same mass spherical particle. The volume moves with the mass weighted sedimentation velocity of its components and at each altitude the atmospheric conditions reflect those of Titan's atmosphere at the same altitude.

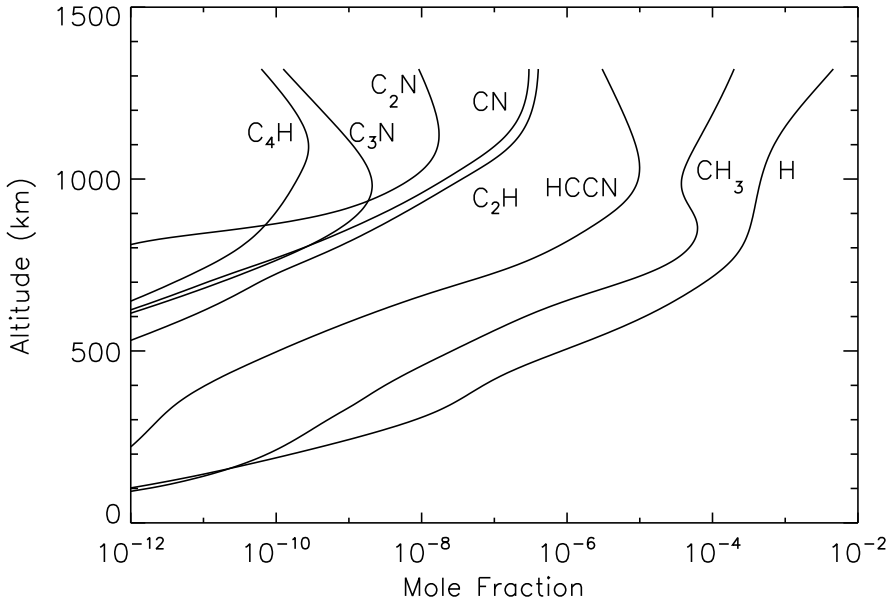

Figure 3: *Radical abundances in Titan's atmosphere from the [19] photochemical model.*

3 Application to Titan

At the low temperature conditions of Titan's atmosphere, reactions among closed cell molecules are inhibited by high energy barriers, and chemical growth proceeds through reactions with radical species. In our calculations we consider the C_2H, CN, and HCCN radical species. Although these are just a few of the anticipated radicals in Titan's atmosphere (Fig. 3), we start our calculations with these three for two main reasons: based on theoretical calculations the first two are expected to have a major role in the growth of PACs, while laboratory experiments suggest that the last has a dominant role in the aerosol production and evolution.

3.1 Gas species

The growth of benzene to larger aromatic structures is known to proceed in combustion chemistry and in the interstellar medium (ISM) were both polycyclic aromatic hydrocarbons and nitrogen containing polyaromatics are observed [1, 14]. The mechanisms involved at these two extreme conditions are different. At high temperatures PACs form through the acetylene addition mechanisms, while at the low temperature conditions of the ISM, aromatic structures grow through ion-molecule reactions (see [4] and references therein). Although the low temperature conditions in Titan's atmosphere do not favor the acetylene addition mechanism, the role of ion-molecule reactions could be important as demonstrated for the formation of benzene in Titan's thermosphere [48]. On the other hand though, the contribution of ions will be

constrained over a narrow altitude region.

Recent laboratory measurements show that the addition of C_2H radicals on benzene is barrierless and proceeds readily at the low temperature conditions of Titan's atmosphere [13]. Furthermore, theoretical calculations suggest that multiple ethynyl additions to a benzene ring lead to the formation of larger aromatic structures [25]. The same is expected for CN addition leading to heterogeneous aromatic structures [16]. Ion chemistry might contribute to the production of aromatic structures from benzene, but the large abundance of the C_2H and CN radicals in Titan's upper atmosphere, combined with their high reaction rate with benzene molecules, suggests that any further growth will be dominated by neutral reactions. Nevertheless, the contribution of ion chemistry in the overall aerosol growth should be investigated in the future.

The choice of HCCN is based on laboratory experiments. Recently, [15] performed laboratory experiments for the photolytic production of Titan aerosol analogs (tholins). In their apparatus they irradiated a N_2/CH_4 gas mixture using tunable VUV radiation at 60 and 82.5 nm, and analyzed both the composition of the resulting gas mixture and the composition of the solid residue produced. The mass spectra of the solid products clearly show the incorporation of nitrogen in the tholins, while the corresponding gas phase spectra demonstrate a lack of nitrogen containing species. This lead [15] to suggest that there is a rapid scavenging of nitrogen by the solid phase. Further analysis of the measured tholin spectra at the two wavelengths of the measurements strongly suggests that the incorporation of nitrogen to the solid phase takes place through mass units corresponding to the HCCN structure. The reaction of HCCN with benzene is not measured yet, but given the high reactivity of this diradical it should also proceed readily.

3.2 Results

The atmospheric gas composition assumed in the calculations is taken from the photochemical model of [19], while for benzene we assume a gaussian production profile located at 1000 km with a width of 12 km and a column production rate of 1.3×10^7 $cm^{-2}s^{-1}$ referred to the surface [48]. The simulation provides a benzene density of 2.5×10^6 cm^{-3} at the top of our simulated atmosphere, consistent with the INMS observations [48, 50]. The benzene molecules grow to larger PACs through reaction with C_2H, CN and HCCN (Fig. 3). We do not keep track of the structure of the formed PACs, we only count the number of C and N atoms in each structure assuming that C and N are equivalent (12 amu). In order to further simplify the calculations, we do not keep track of the H atoms either, since they will have a minor contribution in the overall mass of the particles. Thus, our calculated structures provide a lower limit on the resulting aerosol mass flux.

The main parameters for the calculations are summarized in Table 3.2. The chemical reaction rate of radicals with PACs is taken the same as the rate of C_2H addition of benzene molecules (this is a lower limit since the reaction of C_2H with larger aromatic structures should proceed with a faster rate), while the sticking efficiency

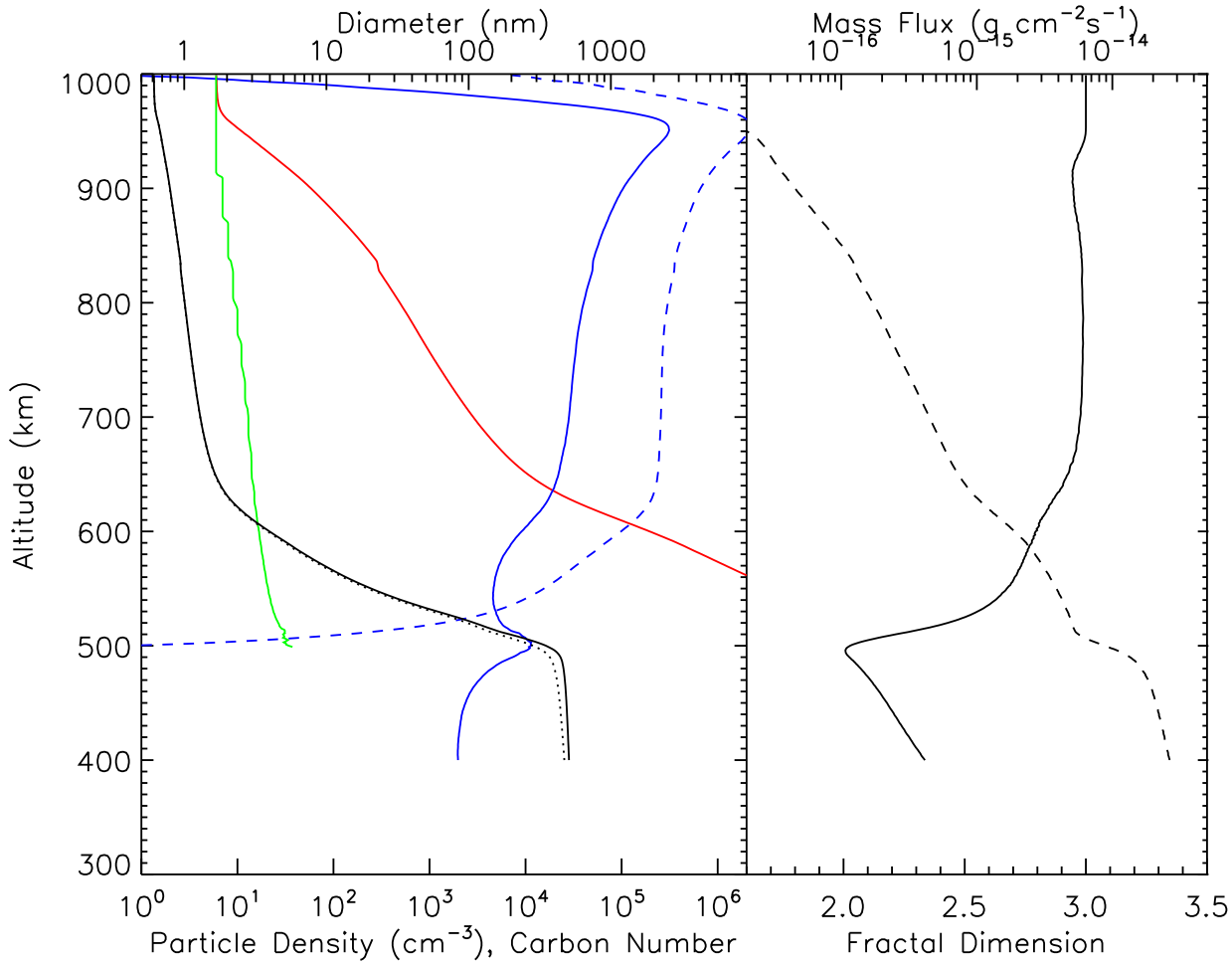

Figure 4: *Overview of main model results for the particle density, size and shape. Left panel: solid and dotted black lines present the average collisional and equivalent sphere diameters, The dashed and solid blue lines are the PAC and particle densities (either primary particles or aerosols), respectively, and the green and red lines are the average number of C atoms in the PACs and particles, respectively. Right panel: The average fractal dimension of the particles (solid line) and the mass flux (dashed line).*

of radicals at the surface of primary particles and aerosols is one (this is different from the sticking efficiency between PACs). The surface smoothing factor, s, on the other hand is not well constrained. For a spherical particle an isotropic mass addition results to a surface geometry factor of two. For aggregates the anisotropy of the system forces the geometry factor to a smaller value due to the presence of the contact points. We first discuss the overall picture of the model results for the case of s=0.75 and afterwards we present a sensitivity analysis on this parameters.

Table 1: *Model parameters*

Parameter		Value
Smoothing parameter	s	0.5-1.5
Surface reaction rate	k_s	3.0×10^{-10} cm^{3}s^{-1}
Charge	q	15 e/μm
Radical sticking efficiency	a_s	1

3.2.1 Nominal Case

Depending on the dominant processes for the production and growth of the average particle mass and shape, we can separate the results into three main altitude regions:

Region I (1000 - 650 km): PAC growth and deposition. The benzene molecules produced close to 1000 km react with the radicals providing the first PACs. The average number of carbon atoms in the PACs is 6 close to the production region (corresponding to benzene molecules), while it increases as the sampling volume moves to lower altitudes, reaching values of ∼40 atoms at 520 km (Fig. 4). The density of PACs remains high in the upper atmosphere and only a small fraction of them provides primary particles (Fig. 4). This is due to the small size of the aromatics that results to a low collision cross section but also to a low sticking efficiency [34].

Assuming that only coagulation affects the shape and size of the produced particles, we should anticipate the formation of aggregates as the generated primary particles fall out of the production region and coagulate with each other. This is reproduced by the model results, as demonstrated by the decrease of the particle fractal dimension, D_f, near 900 km (Fig. 4). On the other hand, D_f increases again shortly below 900 km, and remains close to 3 for altitudes down to ∼650 km. This is a result of the particle surface growth. As shown in Fig. 5, the rates for particle coagulation and PAC deposition are similar in this altitude region, thus, the aggregation of the primary particles is accompanied by the deposition of extra mass on the aerosol surface, that keeps the resulting new particles spherical. The surface growth by direct reaction of the particle's surface with the gas phase radicals also takes place but has a minor contribution (Fig. 5). Hence, the polycyclic aromatics compounds formed in the atmosphere have a dominant role in preserving the spherical shape of the aerosols in the region between the benzene production altitude and ∼650 km. The low atmospheric density in this region allows particles to have a high sedimentation velocity and results in a slow increase of the particle radius in region I. The average

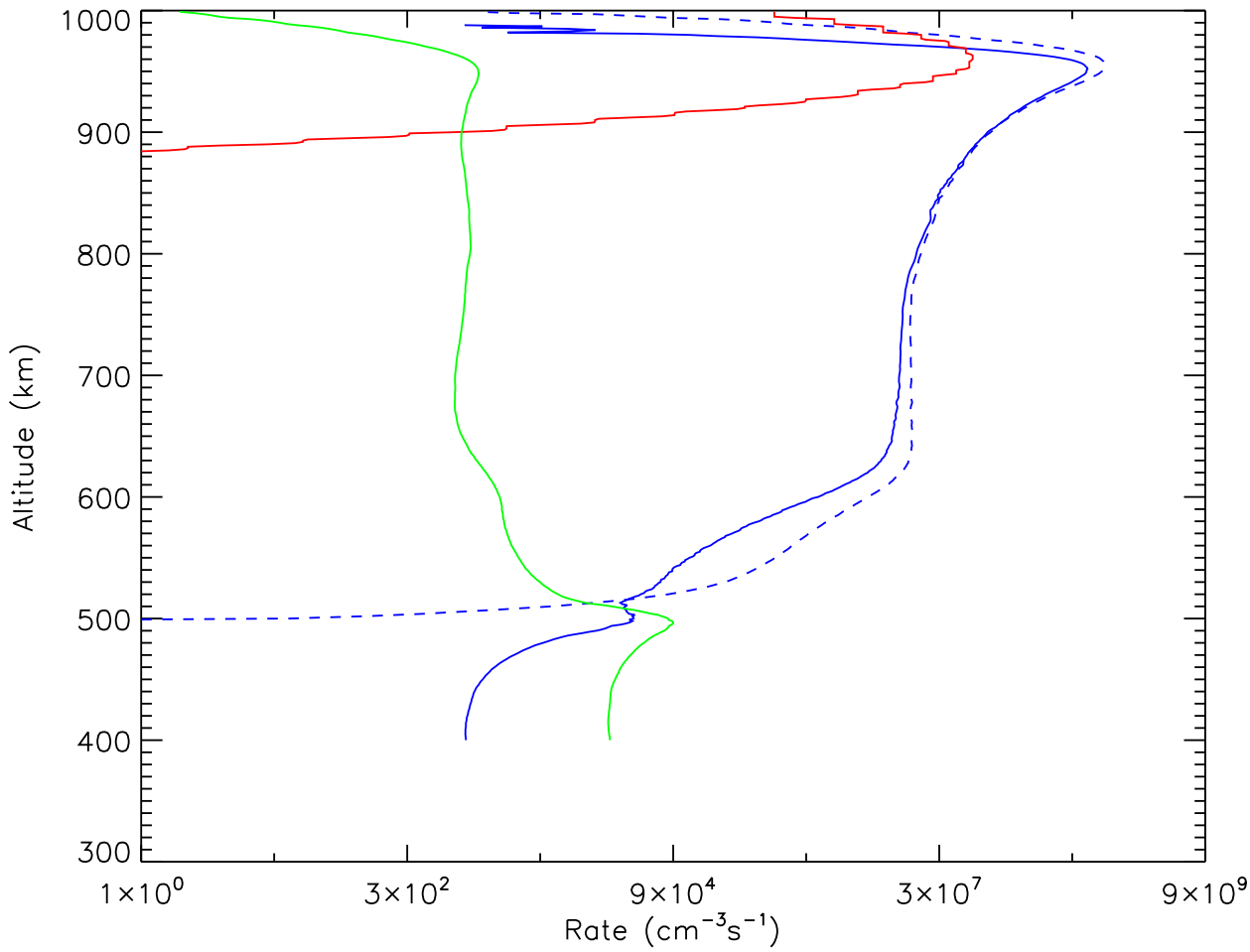

Figure 5: *Comparison of different rates affecting the growth and shape of particles: benzene production (red line), particle coagulation (blue solid line), PAC deposition (blue dashed line) and chemical reaction of radicals on the particle surface (green line).*

collision diameter of the particles ranges between ∼1 nm at 850 km to about 1.7 nm at 650 km.

Thus, the dominant process in region I is the growth of benzene molecules to larger PACs through radical reactions. Simultaneously, the deposition of the aromatic structures on the limited number of aerosols formed, keeps the shape of the particles quasi-spherical.

Region II (650 - 500 km): Particle aggregation. As the average surface of the produced aerosols increases, the loss of PACs due to their deposition on the aerosol surface reduces the abundance of aromatics. This reduction becomes prominent below 650 km, with the number density of aromatics decreasing from $\sim 10^5$ cm^{-3} at this altitude, to 1 cm^{-3} close to 500 km. As a result, the aggregation starts to dominate over the surface smoothing and the particle fractal dimension diverges once again from the spherical limit reaching values close to 2 at 500 km (Fig. 4). The non-spherical shape of the aerosols increases their surface area and collision cross section, therefore, enhances the loss of PACs on their surface and also their coagulation rate. This leads to a rapid growth of the average particle size along with a decrease of the aerosol density. The average collision diameter of the particles increases to 160 nm at 500 km, while the corresponding aerosol density decreases from $\sim 2\times 10^5$ cm^{-3} to $\sim 8\times 10^3$ cm^{-3} between 650 and 500 km.

Another important process affecting the results in this altitude region is the decrease of the average particle settling velocity. Due to the increase of the atmospheric density the particles fall slower relative to the sedimentation velocity at higher altitudes. Furthermore, due to their aggregate structure, aerosols at these pressure conditions are falling with a sedimentation velocity close to the sedimentation velocity of the primary particles composing them, which is smaller than the corresponding velocity of a same mass spherical particle. Therefore, aerosols spend more time in this region, which also contributes to their rapid growth in such a narrow altitude range.

Hence, the reduced surface growth in region II allows for a transition in the aerosols growth mode from spherical to aggregates with a fractal dimension close to 2, while the reduced sedimentation velocity of the aggregates, forces the transition to occur over this narrow region.

Region III (below 500 km): Surface chemistry. At even lower altitudes the model shows an increase of the particle fractal dimension. This results from the surface growth of the aerosols from direct reaction with gas phase radicals. As demonstrated in Fig. 5, the reaction rate of radicals at the surface of aerosols becomes increasingly more important below 600 km and eventually dominates over the coagulation rate. The main radical providing this increase is HCCN that has a high abundance based on the [19] photochemical model. In this altitude region, the high atmospheric density and pressure decreases even further the particle settling velocity. Thus, the sampling volume spends a long time in this altitude region and is furthermore enriched by particles falling from higher altitude. This leads to a pile-up of the particles, demonstrated by the local increase of the particle density right below 500 km. The particle density decreases again at lower altitudes because of the enhanced coagulation rate, which enhances the particle growth (Fig. 4). We

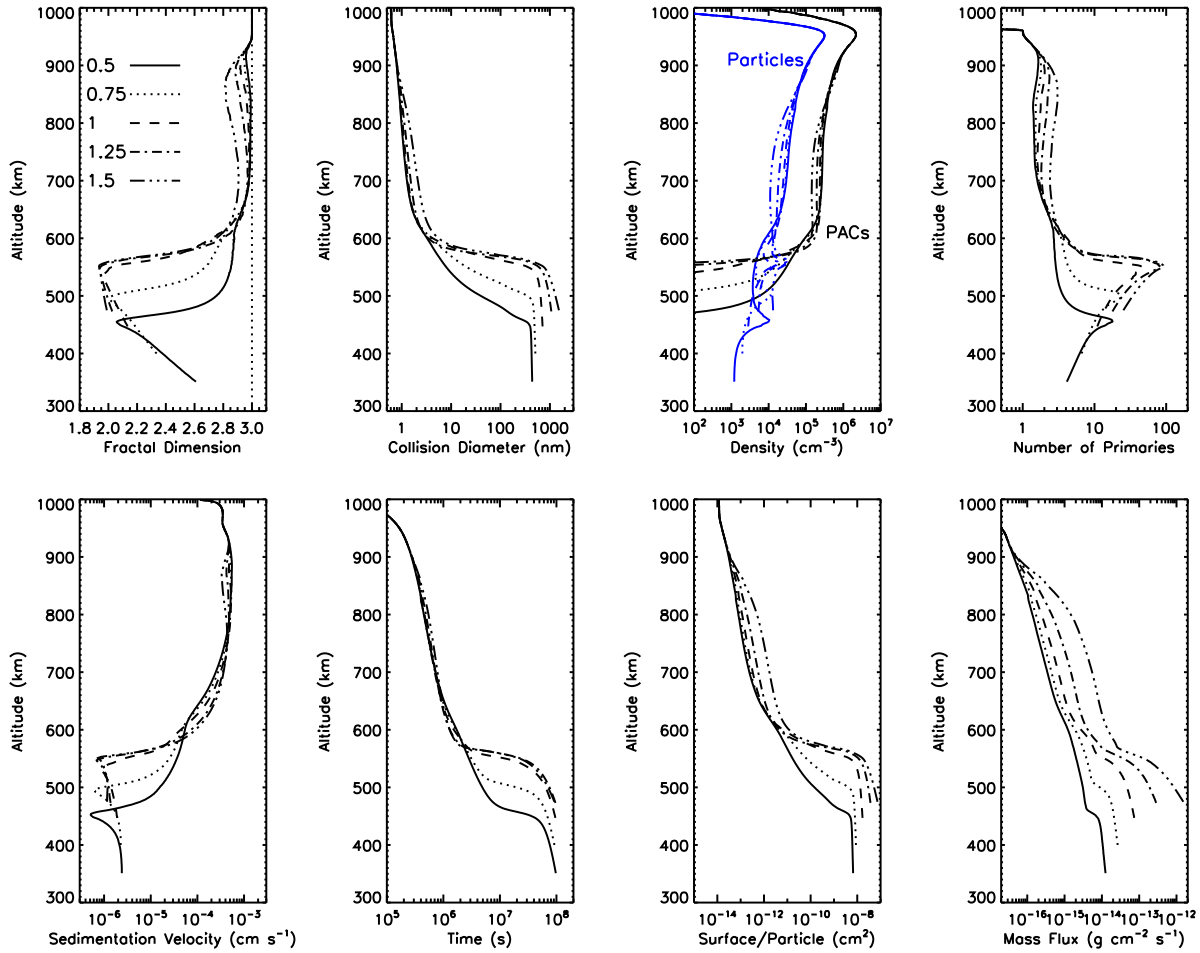

Figure 6: *Sensitivity of model results on smoothing factor. The particle density includes the cumulative contribution of aerosols and PACs.*

should note though that because of the small sedimentation velocity of the particles, the effects of atmospheric mixing and advection are expected to have a larger impact in the aerosol evolution for this region and this is not included in our model.

The above picture of particle evolution demonstrates that not only the particle shape can change depending on the background conditions, but also that the mass flux of particles is changing with altitude. The mass flux at 950 km dominated by the benzene molecules is 2×10^{-17} g cm^{-2}s^{-1} and gradually increase with decreasing altitude, due to the deposition of PACs and radical addition on the surface of aerosols, reaching to $\sim3\times10^{-14}$ g cm^{-2}s^{-1} at the lower boundary of the simulation (Fig. 4).

3.2.2 Sensitivity Analysis

The least constrained parameter in the calculations is the smoothing factor, s, that controls the rounding of the particles due to surface growth. Using different values of s ranging between 0.5 and 1.5, we get a qualitatively similar picture for the

aerosol evolution with the nominal case, but with different results for the final aerosol properties.

For small s values particles get spherical faster than for large s values, for which the aggregate structure of aerosols is better preserved. This is demonstrated by the model results for the average fractal dimension in region I (Fig. 6). The divergence of D_f from the spherical limit becomes increasingly more pronounced as the smoothing factor rises. Nevertheless, for all cases the fractal dimension returns close to the spherical limit (D_f=3), although, at a different altitude that ranges between ∼850 km for s=0.5 and ∼700 km for s=1.5. The departure of particle shape from the spherical limit further affects the size and density of particles. Aggregates have a larger surface area than spherical particles. This translates to a more efficient deposition of PACs and also to an increased coagulation rate due to the increased collision diameter. Therefore, the densities of aromatics and aerosols decrease with increasing values of s, as reproduced by the results. The increase of surface area with increasing s values also enhances the surface growth by radical reaction but with a secondary role in this altitude region relative to the other two processes (coagulation and PAC deposition). Finally the mass flux of aerosols increases with increasing values of s due to the increased surface growth from the deposition of PACs.

In region II, the previous monotonic variation of properties with s becomes more complicated. The aggregation of aerosols depends on the abundance of aromatics, thus, as the PAC density decreases faster with higher s values, the average fractal dimension starts to decrease from 3 at increasingly higher altitudes. This transition altitude is also affected by the sedimentation velocity of the particles. For small s values, particles remain spherical for a longer period, which means that they have a larger sedimentation velocity than the same mass aggregate particles, and are able to penetrate deeper in the atmosphere. This is demonstrated by the variation of sedimentation velocity and altitude with time for the different cases considered (Fig. 6). For s = 0.5 the minimum in the fractal dimension is reached at ∼450 km , while as the s value increases the altitude of minimum D_f shifts to higher altitudes and eventually converges close to 550 km. Hence, the location of the transition altitude for the fractal dimension is defined by the balance between the surface deposition of PACs and the sedimentation velocity of the particles.

At lower altitudes (region III), the aerosol properties are strongly affected by the surface chemistry with the gas phase radicals. For larger s values, the surface area of the particles increases, therefore there is a larger mass addition by the surface chemistry, that generates a larger mass flux of aerosols. This effect is apparent in all the mass flux profiles by the sharp increase in the mass flux in the transition altitude corresponding to region III for each s case. For the largest values of s used in the sensitivity analysis, the resulting mass flux approaches values that are significantly larger than the estimates ($\sim 3\times10^{-14}$ g cm^{-2} s^{-1}) based on Voyager and Cassini observations of Titan's atmosphere [20, 24]. This overestimation of the particle mass flux in this region has to do with the lack of feedback to the gas phase chemistry, i.e. we do not consider the decrease in the gaseous abundances of the radicals as these are lost to the aerosols (this is further discussed below).

Moreover, we assume that the surface chemistry proceeds with a unit efficiency, i.e. any radical hiting the surface of the particles sticks on it. This is an upper limit to the efficiency of surface chemistry and more laboratory measurements are required to set constraints on this parameter for each radical used. On the other hand, for all s values but to a different degree, the added mass contributes in smoothing again the surface of the particles and increasing the average fractal dimension. This becomes increasingly more efficient as s decreases. What we can clearly see is that irrespective of the s value, the fractal dimension transition takes place in a narrow altitude region between 450 and 600 km. This is consistent with the fractal dimension transition suggested to take place at the detached haze layer, based on Cassini observations [20].

It is also interesting to note the different time evolution of the aerosols. We run the simulations for a specific time period (10^8 s). Once aggregates form, particles sediment with the average velocity of the primary particles composing them. Therefore, for all cases considered, the system spends most of its time in the transition region (region II). On the other hand, the different sedimentation velocities of the aerosols (at all altitudes) for different s values, translates to a different maximum penetration altitude for the given simulation time (Fig. 6). This result will be affected by the atmospheric mixing, which is not considered in the current calculations, but it clearly demonstrates how the different processes affecting the shape and size of particles, modify the time particles spend at different altitude regions.

4 Discussion & Conclusions

In the calculations we move the sampling volume of the system according to the sedimentation velocity of its components and we do not include the contribution of atmospheric mixing or diffusion in the resulting particle properties. The impact of this simplification can be investigated by calculating the relative importance of the two processes. The characteristic time for a particle of a given size to sediment the length of a scale height, H, can be estimated as $\tau_s = H/\nu_s$, with ν_s the velocity of the particle. For the same length, the time required to mix the atmosphere is $\tau_m = H^2/K$, with K the eddy mixing coefficient. Using different values for the particle radius and the eddy mixing profile retrieved by photochemical models, we see that sedimentation has a comparable role with atmospheric mixing in the upper atmosphere for the particle sizes retrieved by our calculations, while at lower altitudes the atmospheric mixing dominates (Fig. 7). Thus, the lack of atmospheric mixing should mainly affect the region below 500 km (region III).

Apart from this one dimensional description, atmospheric advection can also affect the resulting particle properties [37]. Advection should be more important at high latitude regions where the closing parts of the Hadley circulation cell components enrich the lower atmosphere with particles from the upper atmosphere (and vice versa for the opposite pole). Furthermore, the impact of horizontal motion will be stronger in the region of the stratospheric jet (close to 300 km), thus, will be mostly affecting region III of our simulation. Therefore our results are representative of

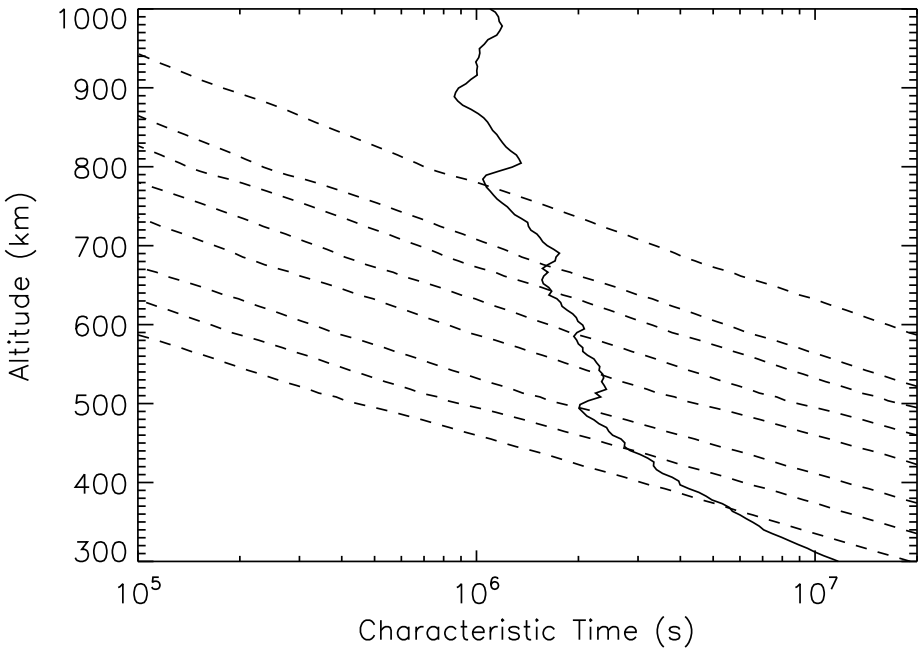

Figure 7: *Characteristic times for atmospheric mixing and sedimentation. The solid line present the characteristic time to mix the atmosphere over a scale height. The structure is due to the use of the observed temperature profile by HASI for the calculation of the scale height. The eddy mixing profile used is taken from the [19] photochemical model. The dashed lines present the characteristic time to settle a scale height for a spherical particle. The different curves correspond to different radius particles with values of 1, 3, 5, 10, 20, 50, 100 and 200 nm from top to bottom.*

conditions at low and mid latitudes, and altitudes above the stratosphere.

We use only a small group of radicals available in Titan's atmosphere for our calculations. Although C_2H, CN and HCCN are among the radicals with the highest abundance, the contribution of other radicals in the growth of PACs and the surface interaction with aerosols can be significant. Among the possible contributors we can point out H_2CN that is a major precursor of HCN on reaction with atomic hydrogen. The abundance of H_2CN is high in the lower atmosphere, thus, if its interaction with the surface of aerosols is efficient, this heterogenous process could affect the vertical mixing ratio of HCN, as suggested in the past in order to explain the divergence of the observed HCN profile from photochemical calculations [17].

We have not coupled the aerosols evolution with the gas phase radical species used in the calculations. This means that we consider the vertical profiles of the radicals unaffected by the aerosol growth. The validity of this assumption depends on the photochemical processes defining the net gas phase production of each species. For example, C_2H and CN are very reactive with other unsaturated hydrocarbons and nitrile species. Therefore their loss is controlled by photochemistry and heteroge-

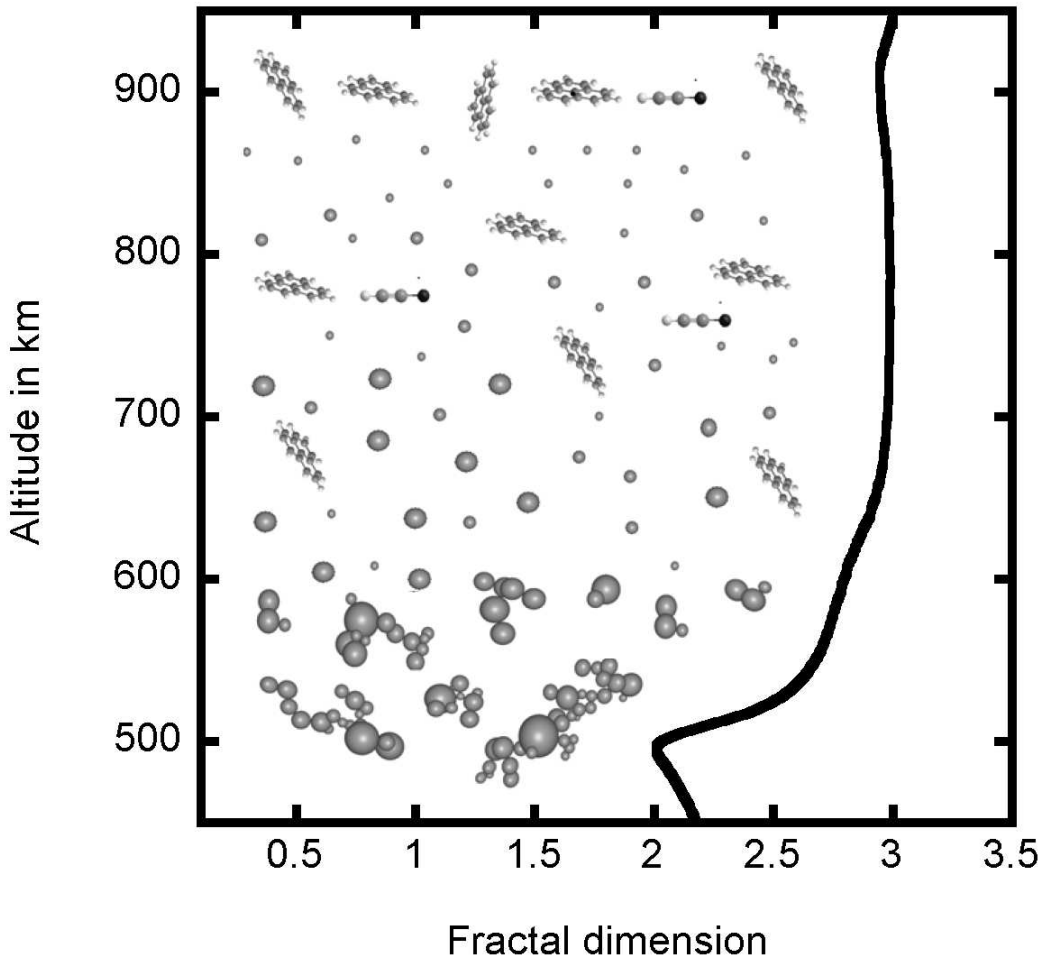

Figure 8: *Shape of the particles at different altitudes.*

neous processes have a minor contribution to their abundance. The photochemical loss processes identified for HCCN are not many. Its main loss identified in photochemical models [18, 54] are self-reaction and reaction with atomic nitrogen to provide C_4N_2 and C_2N_2 respectively. Based on theoretical calculations, [28] also suggested that reaction with H and CH_3 should be important loss mechanisms for HCCN. Inclusion of these reactions to the photochemical model of [19] provides a lower abundance for HCCN's vertical profile, while considering also a heterogeneous loss on the aerosol surface, further decreases its abundance not shown here). Thus, for our current results the impact of the HCCN in the growth of aerosols is an upper limit.

Based on the uncertainties on the abundance of HCCN, as well as, other radicals not included in the calculations, we consider the gas-phase species we include as proxies for the possible contribution of hydrocarbon and nitrogen containing radicals. Our main focus with this investigation is to identify the main processes and mechanisms that can affect the aerosol evolution. Our results demonstrate that the evolution of aerosols in terms of size, shape and density is a result of competing processes between surface growth, coagulation and sedimentation. The particle evolution can be separated into three stages (Fig. 8):

- The benzene molecules produced in the thermosphere react with radical species and grow to bigger aromatic structures. The PACs coagulate and generate the first primary particles, while deposition of the former on the surface of the latter preserves the spherical shape of the particles.
- Once the abundance of PACs is consumed the produced particles aggregate and the average fractal dimension of the system reduces to values close to 2. At the pressure conditions of their formation region, aggregates sediment with a velocity close to the sedimentation velocity of their primary particles. This velocity is significantly smaller than the sedimentation velocity of a same mass spherical particle, thus, aggregates fall slowly. Consequently aggregates grow rapidly over a narrow altitude region.
- As the produced aggregates slowly sediment to lower altitudes, gas-phase radicals are interacting with their surface. Depending on the abundance and sticking efficiency of the radicals the surface of the aggregates is once again smoothed towards a more spherical shape.

The increase of the fractal dimension towards the lower altitudes of our simulation is not consistent with Titan's stratospheric aerosol observations, which clearly show the presence of aggregates with a characteristic fractals dimension of D_f=2 [21, 45]. This is probably a result of the uncertainties in the abundance of HCCN, and also due to the lack of feedback in the gas phase density of radicals used for the surface growth. In addition, the interaction of atomic hydrogen with the aerosol surface will also affect the results in this region. Laboratory experiments find that hydrogenation of the aerosols by incorporation of atomic hydrogen to the aerosol surface is an important process [42], while inclusion of the measured heterogeneous reaction rates to photochemical models [19, 43] shows that this process has its the largest impact

close to 400 km in Titan's atmosphere. Hydrogenation of the aerosols will result to a decrease of the unsaturated bonds in the particle surface, which can affect the sticking efficiency of other radicals and explain why the aerosols in Titan's main aerosol layer in the stratosphere are characteristic of D_f=2. A self-consistent investigation that will couple between the aerosol production and the gas-phase abundances along with the effects of atmospheric mixing and hydrogen heterogenous chemistry will be addressed in the future.

Another clarification we should make is related with the gas to particle transformation pathways. In our calculations we only consider a pathway based on the growth of aromatic structures (homogeneous and heterogeneous polycyclic hydrocarbons), which is based on theoretical calculations for the growth of these structures on reaction with C_2H and CN [16, 25]. Other pathways including both aromatic and aliphatic precursors are suggested in previous investigations based on photochemical considerations [9, 19, 22, 53], but the detailed information for the intermediate steps that will allow the description of these processes in our models are lacking. What we need is a better description of the interaction of large molecules with themselves and also with radicals, in order to identify the possible mechanisms that would provide a stable growth pathway. We hope our current investigation will motivate further theoretical and laboratory investigations that could aid to this goal.

Acknowledgements

This work has been supported through NASA grants NNX09AP14G and NNX09AB58G and NASA's Astrobiology Initiative through JPL subcontract 1372177 to the University of Arizona. MS and MK would like to acknowledge the sup- port from Churchill College and from the EP- SRC (under grant numbers EP/E01772X/1 and EP/G028672/1). PL would like to thank R.V. Yelle for his fruitful comments on the manuscript.

References

[1] Allamandola, L.J., Tielens, A.G.G., Barker, J.R., 1989. Interstellar polycyclic aromatic hydrocarbons: The infrared emission bands, the excitation/emission mechanism, and the astrophysical implications. Ap.J. Supp., 71,733-775.

[2] Appel,J., H. Bockhorn, and M. Frenklach. Kinetic modeling of soot formation with detailed chemistry and physics: Laminar premixed flames of C2 hydrocarbons. Com- bust. Flame, 121:122136, 2000. doi:10.1016/S0010-2180(99)00135-2.

[3] Balthasar, A., Kraft, M., 2003. A stochastic approach to calculate the particle size distribution function of soot particles in laminar premixed flames. Comb. and Flame 133, 289-298.

[4] Bauschlicher, C.W.,Jr, Ricca, A., 2000. Mechanisms for polycyclic aromatic hydrocarbons (PAH) growth. Chem. Phys. Lett., 326, 283-287.

[5] Celnik, M.S., Sander, M., Raj, A., West, R.H., Kraft, M., 2009. Modelling soot formation in a premixed flame using an aromatic-site soot model and an improved oxidation-rate. Proc. Comb. Inst., 32, 639-646.

[6] Celnik, M.S., Patterson, R.I.A., Kraft, M., Wagner, W., 2010. A predictorcorrector algorithm for the coupling of stiff ODEs to a particle population balance.J. Comput. Phys. 228, 2758-2769.

[7] Coates, A.J. Crary, F.J., Lewis, G.R., Young, D.T., Waite, J.H. Jr., Sittler, E.C. Jr., 2007. Discovery of heavy negative ions in Titan's ionosphere. Geoph. Res. Let., 34 , L22103.

[8] Crary, F.J., Magee, B.A., Mandt, K., Waite, J.H. Jr., Westlake, J., Young, D.T., 2010. Heavy ions, temperatures and winds in Titan's ionosphere: Combined Cassini CAPS and INMS observations. PSS, 57, 1847-1856.

[9] Delitsky, M.L., and McKay, C.P., 2010. The photochemical products of benzene in Titan's upper atmosphere. Icarus, 207, 477-484.

[10] Eibeck, A., Wagners W., 2000. Approximative solution of the coagulation-fragmentation equation by stochastic particle systems. Stochastic Anal. Appl. 18, 921-948.

[11] Frenklach,M. and H. Wang. Detailed Mechanism and Modelling of Soot Particle Formation, volume 59 of Series in Chemical Physics, pages 162190. Springer Verlag, Berlin, 1994.

[12] Goodson, M., Kraft, M., 2002. An efficient stochastic algorithm for simulating nano-particle dynamics. JOURNAL OF COMPUTATIONAL PHYSICS 183, 210-232.

[13] Goulay, F., Leone,, S.R., 2006. Low-temperature rate coefficients for the reaction of ethynyl radical (C_2H) with benzene. J. Phys. Chem. A., 110, 1875-1880.

[14] Hudgins, D.M., Bauschlicher, C.W., Allamandola, L.J., 2005. Variations in the peak position of the 6.2 μm interstellar emission feature: a tracer of N in the interstellar polycyclic aromatic hydrocarbon population. Ap.J., 632,316-332.

[15] Imanaka, H., Smith, M.A., 2010. Formation of nitrogenated organic aerosols in the Titan upper atmosphere. PNAS, *inpress*.

[16] Landera, A., Mebel, A.M., 2010. Mechanisms of formation of nitroge-containing polycyclic aromatic compounds in low-temperature environments of planetary atmospheres: A theoretical study. Faraday Discuss., 147, DOI: 10.1039/c003475d.

[17] Lara, L.-M., Lellouch, E., Shematovich, V., 1999. Titan's atmospheric haze: the case of HCN incorporation. Astr. Astrophys., 341, 312-317.

[18] Lavvas, P.P., Coustenis, A., Vardavas, I.M., 2008a. Coupling photochemistry with haze formation in Titan's atmosphere. Part I: Model description. Planet. Space Sci., 56, 27-66.

[19] Lavvas, P.P., Coustenis, A., Vardavas, I.M., 2008b. Coupling photochemistry with haze formation in Titan's atmosphere. Part II: Results and validation with Cassini/Huygens data. Planet. Space Sci., 56, 67-99.

[20] Lavvas, P., Yelle, R.V., Vuitton, V., 2009. The detached haze layer in Titan's mesosphere. Icarus, 201, 626-633.

[21] Lavvas, P., Yelle, R.V., Griffith, C.A., 2010. Titan's vertical aerosol structure at the Huygens landing site. in press, doi:10.1016/j.icarus.2010.07.025

[22] Lebonnois, S., E.L.O. Bakes and C.P. McKay (2002). Transition from gaseous compounds to aerosols in Titan's atmosphere. Icarus 159, 505-517.

[23] Liang, M-C., Yung, Y.L., Shemansky, D.E., 2007. Photolytically generated aerosols in the mesosphere and thermosphere of Titan. Astrophys. J., 61, L199-L202.

[24] McKay, C.P., Coustenis, A., Samuelson, R.E., Lemmon, M.T., Lorenz, R.D., Cabane, M., Rannou, P., Drossart, P., 2001. Physical properties of the organic aerosols and clouds on Titan. Planet. Space Sci., 49, 79-99.

[25] Mebel, A.M., Kislov, V.V., Kaiser, R.I., 2008. Photoinduced mechanism of formation and growth of polycyclic aromatic hydrocarbons in low-temperature environments via successive ethynyl radical additions. JACS, 130, 1361813629.

[26] Mitchell, P., Frenklach, M., 2003. Particle aggregation with simultaneous surface growth. Phys. Rev. E., 67, 061407, DOI: 10.1103/PhysRevE.67.061407

[27] Morgan, N., Kraft, M., Balthasar, M., Wong, D., Frenklach, M., Mitchell, P., 2007. Numerical simulations of soot aggregation in premixed laminar flames. Proc. Comb. Inst., 31, 693-700.

[28] Osamura, Y., Petrie, S., 2004. NCCN and NCCCCN formation in Titan's atmosphere: 1.Competing reactions of precursor HCCN ($^3A''$) with H(^2S) and CH_3($^2A'$). J. Phys. Chem. A, 2004, 108, 3615-3622.

[29] Patterson, R.I.A., Singh, S., Balthasar, M., Kraft, M., 2006. The Linear Process Deferment Algorithm: A new technique for solving population balance equations. SIAM Journal on Scientific Computing 28, 303-320.

[30] Patterson,R. I. A. and M. Kraft. Models for the aggregate structure of soot particles. Combust. Flame, 151:160172, 2007. doi:10.1016/j.combustflame.2007.04.012.

[31] Porco et al., 2005. Imaging of Titan from the Cassini spacecraft. Nature, 434, 159-168.

[32] Pratsinis, S. E., 1988. Simultaneous nucleation, condensation, and coagulation in aerosol reactors. J. Colloid Interface Sci., 124:416428, 1988. doi:10.1016/0021-9797(88)90180-4.

[33] Rages, K., Pollack, J.B., Smith, P.H., 1983. Size estimates of Titan's aerosols based on Voyager high-phase-angle images. J. Geophys. Res., 88, 8721-8728.

[34] Raj, A., M. Sander, V. Janardhanan, and M. Kraft. A study on the coagulation of polycyclic aromatic hydrocarbon clusters to determine their collision efficiency. Combustion and Flame, 157, 523-534.

[35] Rannou, P., Cabane, M., Chassefiere, E., Botet, R., McKay, C.P., Courtin, R., 1995. Titan's geometric albedo: Role of the fractal structure of the aerosols. Icarus, 118, 355-372.

[36] Rannou, P., C.P. McKay and R.D. Lorenz, 2003. A model of Titan's haze of fractal aerosols constrained by multiple observations,Planet. Space Sci., 51, 963-976.

[37] Rannou,P., Hourdin, F., McKay, C.P., Luz, D., 2004. A coupled dynamics microphysics model of Titan's atmosphere. Icarus, 170,443-462.

[38] Sander M., Patterson, R. I. A., Raj, A., Kraft M., 2010. Comment on Low Fractal Dimension Cluster-Dilute Soot Aggregates from a Premixed Flame. Phys. Rev. Lett 104, 119601.

[39] Sander M., Patterson, R. I. A., Braumann A., Raj, A., Kraft M. Developing the PAH-PP soot particle model using process informatics and uncertainty propagation, 2010. Proc. Combust. Inst. 33.

[40] Sander M., West R. H., Celnik M. S., Kraft M., 2009. A Detailed Model for the Sintering of Polydispersed Nanoparticle Agglomerates. Aerosol Sci. Technol. 43, 978-989.

[41] Sander M., Raj A., Inderwildi O. R., Kraft M., Kureti S., Bockhorn H., 2009. The simultaneous reduction of nitric oxide and soot in emissions from diesel engines.Carbon 47, 866-875.

[42] Sekine, Y., Imanaka, H., Matsui, T., Khare, B.N., Bakes, E.L.O., McKay, C.P., Khare, B.N., Sugita, S., 2008. The role of organic haze in Titan's atmospheric chemistry I. Laboratory investigation on heterogeneous reaction of atomic hydrogen with Titan tholin. Icarus, 194, 186-200.

[43] Sekine, Y., Lebonnois, S., Imanaka, H., Matsui, T., Bakes, E.L.O., McKay, C.P., Khare, B.N., Sugita, S., 2008. The role of organic haze in Titan's atmospheric chemistry II. Effect of heterogeneous reaction to the hydrogen budget and chemical composition of the atmosphere. Icarus, 194, 201-211.

[44] Tomasko, M.G., and Smith, P.H., 1982. Photometry and polarimetry of Titan: Pioneer 11 observations and their implications for aerosol properties. Icarus, 51, 65-95.

[45] Tomasko, M.G., Doose, L., Engel, S., Dafoe, L.E., West, R., Lemmon, M., Karkoschka, E., See, C., 2008. A model of Titan's aerosols based on measurements made inside the atmosphere. Planet. Space Sci., 56, 669-707.

[46] Totton, T.S., Chakrabarti, D., Misquitta, A.J., Sander, M., Wales, D.J., Kraft, M., 2010. Modelling the internal structure of nascent soot particles. Comb. and Flame 157, 909-914.

[47] Vuitton V., Yelle, R.V., McEwan, M.J., 2007. Ion chemistry and N-containing molecules in Titan's upper atmosphere. Icarus, 191, 722-742.

[48] Vuitton V., Yelle, R.V., Cui, J., 2008. Formation and distribution of benzene on Titan. J. Geophys. Res., 113, 10.1029/2007JE002997

[49] Waite, J.H.Jr., and 21 co-authors, 2005. Ion neutral mass spectrometer results from the first flyby of Titan. Science, 308, 982-986.

[50] Waite, J.H.Jr., Young, D.T., Cravens, T.E., Coates, A.J., Crary, F.J., Magee, B., Westlake, J., 2007. The process of tholin formation in Titan's upper atmosphere. Science, 316, 870-875.

[51] West, R.A., and 8 co-authors, 1983. Voyager 2 photopolarimeter observations of Titan. J. Geophys. Res., 88, 8699-8708.

[52] West, R.A., and Smith, P.H., 1991. Evidence for aggregate particles in the atmospheres of Titan and Jupiter. Icarus, 90, 330-333.

[53] Wilson, E.H. and S.K. Atreya (2003). Chemical sources of haze formation in Titan's atmosphere. Planet. Space Sci. 51, 1017-1033.

[54] Yung, Y. L., Allen, M., Pinto J.P., 1984. Photochemistry of the atmosphere of Titan: Comparison between model and observations. Astrophys. J. Supp. 55, 465-506.